Leveraging compliance in origami robot legs for robust and natural locomotion

X. Deng, C. Sung

Abstract: *We present an origami-inspired compliant robot leg design with three degree of freedom compliance. Using the proposed leg, we created a full quadrupedal robot that can walk robustly with adaption to non-flat terrains and external perturbations. We can reconfigure the design to change the stiffness. According to systematic locomotion tests, we demonstrate unique advantages of the proposed leg design over a rigid counterpart of the same dimension and weight in terms of enhancing locomotion stability.*

1 Introduction

Making legged robots walk and run like humans and animals has been a challenging task of robotics research. During walking and running, humans and animals take advantage of compliance in their tendons and muscles to periodically store and release energy so as to achieve stable and energy-efficient gaits. In this case, stiffness is the key parameter that characterizes the bouncing motion by associating the ground reaction force with leg compression.

Legged robot designs that similarly make use of elastic energy in this way have demonstrated greater robustness and efficiency of locomotion [Saranli et al. 01, Li et al. 12, Mintchev et al. 17] than their rigid counterparts. However, these designs are often complex and take quite a bit of effort to produce. In contrast, origami-inspired robots are able to naturally incorporate compliant mechanisms while being relatively fast to fabricate. Furthermore, origami-inspired robots have unique advantages in terms of their lightness, low cost, and re-configurable features, which in turn can make origami-inspired robots more accessible for prototyping and design investigation [Rus and Sung 18].

Origami mechanisms are compliant mechanisms [Rommers et al. 17]. Origami panels and hinges can store energy through deflection under external forces, resulting in spring forces that resist perturbations and restore from deformations [Greenberg et al. 11]. Such energy restoration and release mechanisms offer the potential of improved locomotion stability. Unfortunately, among the to-date origami-inspired legged robot research, the intrinsic compliance properties of origami have been rarely incorporated into the dynamical capability of origami-inspired robots in a systemic design approach. Existing work on achieving dynamical locomotion capabilities such as crawling and jumping [Onal et al. 13, Zhakypov et al. 17, Noh

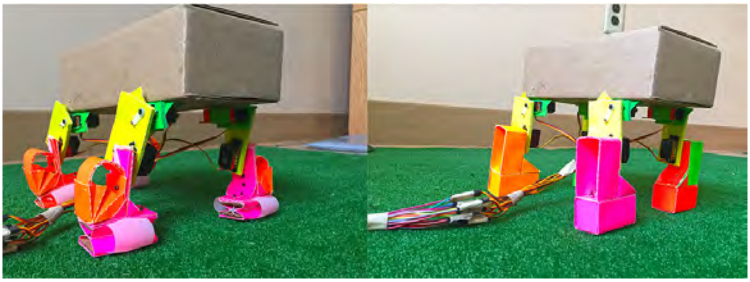

Figure 1: *Our origami-inspired quadruped robot design with the proposed compliant legs (left) vs. rigid legs (right).*

et al. 12] have focused on using shape-changing smart actuators, especially shape memory alloys (SMA) actuators, on top of origami joints, i.e. hinges, to generate elastic power and motions. Yet, among these studies, 1) origami joints are often assumed as otherwise static and passive [Zhakypov and Paik 18]—that is, smart actuators are considered as the major source of elastic energy; and 2) the characterization of these shape-changing actuators involves complex factors including multi-layer, multi-material compositions, heaters and geometry which in turn imposes challenges to design [Zhakypov and Paik 18].

At the same time, computational design and fabrication tools have shown promising progress in making origami-inspired robots with any form and kinematics [Soltero et al. 13, Schulz et al. 17]. Using pattern composition algorithms for parameterized origami joints [Sung and Rus 15] and bodies, origami-inspired robots with any shape and movement can be composed and fabricated in a print-and-fold fashion. However, progress in this area still relies on rigid body assumptions for kinematic analysis and is limited in incorporating parameterized models of the compliance properties of origami into computational tools.

1.1 Contributions

In this paper, we take advantage of the intrinsic compliance of origami to create a leg design with enhanced locomotion stability. Inspired by a dynamical template of animal's running in [Holmes et al. 06], we have developed a compliant origami robot leg with the following objectives: 1) The leg adapts to unforeseen physical interactions and uneven terrains; 2) The adaption to physical collisions reduces unexpected impacts in comparison to stiff legs; and 3) Nonexpert designers without technical backgrounds can easily design and fabricate the legs for their robotics applications. In this paper, we describe our leg design that satisfies these objectives, and we present parameterized designs that allow users to specify body structure and stiffness for their particular application. We integrate these designs into a fabricated quadruped and show that the compliant legs increase stability and reduce impact forces on the robot.

This paper is organized as follows. Section 2 introduces dynamic modeling

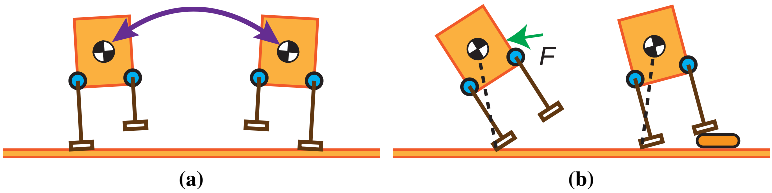

Figure 2: *(a) Lateral view of normal gait cycle: the center of mass is periodically moving towards the stance foot (feet); (b) Perturbed center of mass dynamics due to external pushes or collisions with obstacles can be approximated by a perturbed inverted pendulum model.*

behind running and walking gaits and the expected effect of compliance on these behaviors. Section 3 describes our compliant origami leg design. Section 4 shows an example of this leg design incorporated into a quadrupedal robot. Section 5 provides force and stability measurements on the resulting design. Section 6 concludes with directions for future work.

2 Dynamic Model of Robot Locomotion

Understanding a legged robot's three dimensional body dynamics during a gait cycle is essential for practical considerations of leg design. A key question is how to design the passive dynamics of compliant legs in a way that enhances the robustness of locomotion to external perturbations. Existing literature has shown that spring-like legs are essential for running in most animals [Blickhan and Full 93]. As a result, the spring-loaded inverted pendulum model (SLIP) is a model [Holmes et al. 06] commonly used to describe the normal body movement of a running animal as a point mass bouncing on an elastic leg. Based on this model, we can take advantage of elasticity and damping in the mechanical design of a robotic leg for balanced locomotion against external disturbances.

In general, the full body dynamics of legged locomotion can be decomposed into the sagittal (left-right) and lateral (back-front) directions. We first consider the lateral direction. Fig. 2a depicts the lateral view of a rigid legged robot's oscillation as its feet periodically lift off and touch down. As swing and stance feet switch, the center of mass (CoM) shifts periodically towards the current stance foot to maintain balanced foot steps. Upon external perturbations as shown in Fig. 2b, when a rigid robot is pushed or steps on obstacles, the perturbed CoM dynamics can be approximated as a perturbed linear inverted pendulum (LIPM) regardless of the number of legs. In such cases, the CoM rotates around the lowest contact edge between the robot and the ground; this edge can be viewed as the pivot of a LIPM.

In general, the dynamical system of a one dimensional LIPM can be written as

$$\dot{\chi} = B\chi, B = \begin{bmatrix} 0 & 1 \\ C & 0 \end{bmatrix} \tag{1}$$

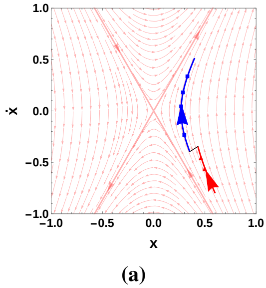

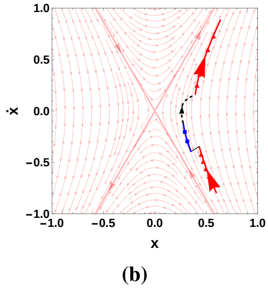

Figure 3: *(a) perturbed dynamics of a LIPM visualized on phase plane: red (with triangle markers) trajectory with lower constant orbital energy—before perturbation; blue (with square markers) trajectory with higher orbital energy—after perturbation; (b) orbital energy recovery through temporally augmented external control (black dashed)*

with $C = \sqrt{g/h} \in \mathbb{R}^+ and \chi = (x, \dot{x})^T \in \mathbb{R}^2$, where g is the gravity, h is the CoM height, and x is the position of the CoM with respect to the pendulum pivot. Eqn. (1) has the following time invariant property:

$$\begin{aligned} E_0 &= \dot{x_0}^2 - Cx_0^2 \\ &= \dot{x_t}^2 - Cx_t^2 \end{aligned} \tag{2}$$

with $\chi_t = (x_t, \dot{x_t})^T = e^{Bt}\chi_0$ for any initial state $\chi_0 = (x_0, x_0)^T$, $t \in \mathbb{R}$. E_0 is called orbital energy.

Eqn. (2) states that for an unperturbed LIPM, its orbital energy will remain constant in time. In other words, if a LIPM state is perturbed, the natural dynamics of the LIPM can not recover the orbital energy (corresponding to an invariant set of states satisfying eqn. (2) for a given E_0) before the perturbation. We can visualize the perturbation effect on the phase plane Fig. 3a, where the red line represents the initial unperturbed trajectory and the blue line represents the trajectory after a simulated instantaneous state modification of $\delta\chi = (-0.08, -0.05)^T$. The light red lines indicate equivalent energy stages

Fig. 3b shows the orbit recovery in comparison to Fig. 3a, where the dashed black line indicates a continuous state recovery effort from the perturbed (blue) trajectory to the nominal (red) trajectory. The approach in orbit recovery shown in Fig. 3a was detailed in [Deng and Lee 18], which added temporal augmented dynamics to the passive dynamics of a LIPM. The form of the temporal dynamical system can be written as

$$\dot{\chi} = B\chi, B = \begin{bmatrix} 0 & 1 \\ C - K(E) & -D(E) \end{bmatrix} \tag{3}$$

with $K(E) < C, D(E) \in \mathbb{R}_0^+$. If $K > 0, D > 0$, then the augmented temporal dynamics correspond to a virtual damped harmonic oscillator system. That is, recovery

(a) (b) (c)

Figure 4: *Compliant leg. (a) Bending panels with folding structures to make compliance reconfigurable; (b) bending structure with reconfigurable compliance added to the proposed leg design; (b) side view of the leg*

from perturbation is possible if the interactions between the CoM and stance leg resembles a damped harmonic oscillator. In light of this conclusion, our goal is to design spring and damper functionalities in compliant origami robotic legs in order to achieve the dynamical resistance to perturbations in locomotion.

Note that although our analysis in this section is regarding the lateral dynamics, similar analysis applies to the sagittal dynamics. This is because in either direction we assume that when a rigid robot being pushed, its body will tilt about the lowest foot edge that is in contact with the ground.

3 Origami Design

To embed damped harmonic oscillator dynamics into an origami leg design, we target three objectives: elastic foot touch-down during normal gait, adaptation to uneven terrains, and lateral and sagittal balancing against physical perturbations. Fig. 4 and Fig. 5 show our final design. The leg consists of a compliant ankle and foot with a bending lower leg, an attachable module for compliance control, and a rigid upper leg. The diagram in Fig. 6 shows the types of deformations achievable with this leg design. From a high level perspective, the designed actuations resemble two common dynamical templates: a spring-loaded pendulum and a torsion spring. The combined design allows automatic whole leg adjustments to physical interactions at the foot or body while reducing impacts compared to a rigid leg.

Leg Stiffness. Our overall strategy to compliance is to use bending faces to control the stiffness of our designs. Fig. 7 shows a cross-sectional view of our joints (detailed in the following sections) in orange, with blue lines corresponding to external bending components. The bent material results in a spring-like restoring force that pushes the joint to its equilibrium position. The restoring force increases with the magnitude of deflection, and the stiffness of these faces depends on their length and material thickness. Joint stiffness can thus be adjusted by adjusting face lengths during the design phase or through on-site active control.

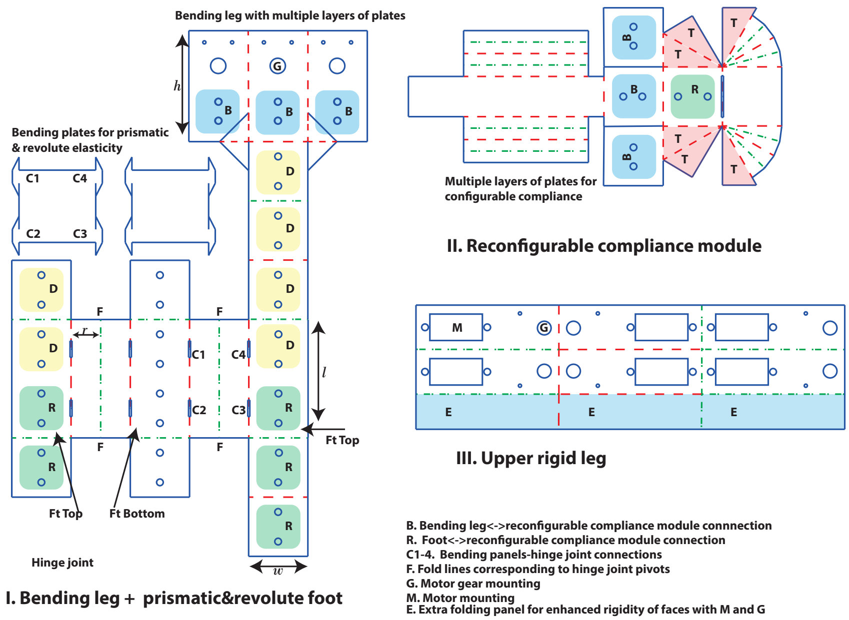

Figure 5: *Fold pattern for compliant leg. Dashed lines are valley folds, dashed-dotted lines are mountain folds, and solid lines are cuts. Shaded regions of the same color are glued together when the leg is assembled. Letters indicate connected faces and edges on the pattern.*

3.1 Compliant foot

Ankle design and ankle stiffness are critical for human and animals in terms of balancing and adaptation to uneven surfaces [Roy et al. 09]. At the same time, compliance along the direction of foot touch-down is important for impact force reduction as well as energy restoration prior to leg swing. Our foot design combines these two considerations into a two degree-of-freedom foot design with both translational and bending compliance. The bottom portion of Fig. 5(I) shows the fold pattern for the compliant foot. Fig. 7a is the cross-sectional view of this design. The yellow shaded region, the black dots and the green arrows correspond to the interior of the joint, the fold lines, and the directions of spring forces, respectively. The joint structure breaks down into two folded panels in parallel. Symmetric folding of the panels produces translational motion and linear restoring forces, similar to a one-dimensional spring. Asymmetric folding of the panels produces a rotational motion and a bending moment for foot tilt. The purple dot is the virtual axis of rotation, which may move depending on the fold angles for the two panels.

Each of the folds can be modeled as a torsion spring [Dai and Cannella 08,Sung and Rus 15] with some equilibrium fold angle. For small angles, the stiffness of this hinge joint is proportional to the angular displacement from the nominal joint

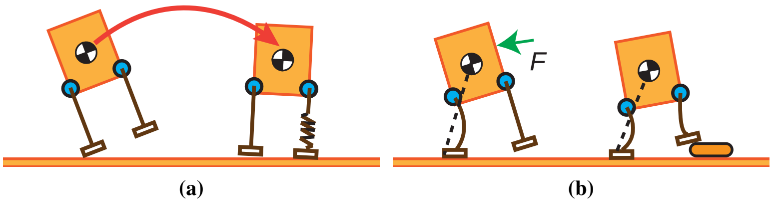

Figure 6: *(a) Adding elasticity to the foot reduces touch-down impacts when the CoM moves towards the new stance foot after perturbations; (b) Adding compliance to leg produces hip torques counteracting external perturbations.*

angle. However, relying on the compliance of the fold itself can be restrictive. Due to repetitive rotations, the forces acting on a single fold line can easily cause a decrease of stiffness of the rotational fold. The bending panels (blue lines) are therefore added for practical considerations. The deformed ring can help the ankle to gain extra supporting force from an uneven terrain. In addition, changing the lengths of the bending panels allows finer control over the foot stiffness. Finally, the bending panels help with fold fatigue by distributing the resistance forces to other places on the ring.

Force analysis As [Dai and Cannella 08, Sung and Rus 15], we model the hinge joints as torsion springs. Denote ϕ as the fold angle, ϕ_1^0 and ϕ_2^0 as angles of the two folds at equilibrium state, ϕ_1 and ϕ_2 as the fold angle (ref. Fig. 7b) after twisting, and k_1 and k_2 as the spring's torsion coefficients. We approximate the torque of the folds as

$$\tau_{hinge} = -k_1(\phi_1 - \phi_1^0) - k_2(\phi_2 - \phi_2^0) \tag{4}$$

where the stiffness varies proportionally to the fold length and to the cube of material thickness.

The bending panels also restoring forces. Similarly to [Faal et al. 16], we use deflection equations of cantilever beams to approximate the forces as linear. Let θ denote the deflection angle, the angle between the tangent line of a bending panel at a chosen pivot and the horizontal line, θ_0 be the deflection angle at the equilibrium state before an external force is applied, θ_1 be the deflection angle after an external force is applied, L be the bending panel length, E be the elastic modulus of the material, and I be the area moment of inertia of the bending panel about the rotation axis. When the deflection $(\theta_1 - \theta_0)$ is small, the force produced by one bending panel can be computed as:

$$F = 8EI\sin(\theta_1)\frac{(\theta_1 - \theta_0)}{L^2} \tag{5}$$

where $I \propto l_f t^3$ where l_f is the length of the fold and t is the material thickness.

Both of these forces contribute to translational restoring forces and rotational restoring torques on the foot. We can compute the forces F_1 and F_2 acting on either

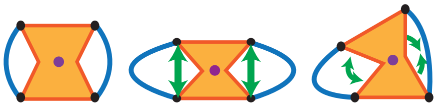

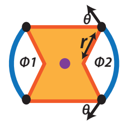

Figure 7: *(a) Two degree-of-freedom foot with prismatic and revolute compliance; (b) Parameters for the foot*

side of the joint. Then given the radius of each hinge joint r, a portion of the forces contribute to rotation, and the torque due to bending is

$$\tau_{bend} = \tau_{hinge} + \alpha \left(rF_1 \cos\frac{\phi_1}{2} - rF_2 \cos\frac{\phi_2}{2} \right) \tag{6}$$

where $\alpha = 1$ if $\phi_1 < \phi_2$, $\alpha = -1$ if $\phi_1 > \phi_2$ and $\alpha = 0$ if $\phi_1 = \phi_2$

This net restoring torque is depending on the size of the joint, the lengths of the bending panels, the thickness of the material, and the elastic modulus of the material. Practically, the forces from the bending panels tend to dominate over the forces from the folds. It is therefore possible to increase the stiffness of the foot by increasing the thickness or shortening the lengths of the bending panels.

3.1.1 Bending leg for lateral balancing

During normal gait cycles, the center of pressure must periodically shift towards the stance feet in order to ensure stable foot stepping in the sagittal direction. Therefore, maintaining lateral balance is crucial for legged locomotion. Our compliant leg design aims to achieve the following sub-objectives: 1) less CoM deviation under the same amount of external disturbances in the lateral direction than the rigid counterpart; 2) the compliant mechanism should automatically resist perturbations to the CoM and re-balance the robot's body once the external force is relaxed; and 3) the compliant mechanism should help maintain the contact area between the stance foot and ground when the CoM is perturbed.

Our leg design uses the elasticity properties in bending panels to meet the objectives above. The top portion of Fig. 5(I) shows the fold pattern for the compliant leg. Fig 8a (left) shows the conceptual idea of the bending leg design: through deflection, the leg produces resisting forces on the hip joint to counterbalance the CoM while adapting the ankle angle to maintain foot contact area. The usage of the hip joint for lateral balancing also aligns with existing studies in human balance during walking which has shown the dominant importance of hip for lateral balancing based on observed joint torques [Winter 95, Matjačić et al. 01]. Fig. 8a and Fig. 8b are the sagittal and lateral views, respectively, of the bending leg integrated with the compliant foot.

Force analysis Given the deflection angle—the angle between the tangent line of the bending leg at its hip pivot and the vertical is defined as θ, θ_1 denotes the

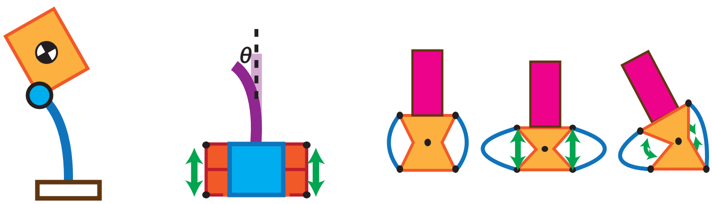

(a) (b)

Figure 8: *(a) Modeling of the bending leg (left) and sagittal view of the composition of the bending leg and the compliant foot. (b) Lateral view of the bending leg and compliant foot composition*

deflection angle after external force applied, L the bending panel length, E the elastic modulus of the material and I the area of moment inertia of the bending panel about the rotation axis. The net force normal to the bending panel at the hip joint can be computed as:

$$F_{hip} = \frac{2\theta_1 EI}{L^2} \tag{7}$$

Therefore, similarly to the compliant foot, it is possible to increase the stiffness of the leg by increasing its thickness or decreasing its length.

3.2 Augmented reconfigurable compliance

Finding optimal parameters for the compliant leg design is difficult because the performance of the leg is inherently sensitive to modeling accuracy and the magnitude of external disturbances. Due to the nonlinearity and complexity in the compliant elements, it is valuable to add reconfigurability of the compliance in the fabricated leg so that users can adjust the leg compliance in different real-world scenarios.

We therefore add a folding structures to the leg. The module consists of a ring of bent material constrained inside a collapsible box. Fig. 5 (II) shows the folding pattern of the reconfigurable compliant module, and Fig. 4 shows the folded state. Changing the number of pleats on the ring changes its minimum stiffness. By collapsing pleats on the side of the box, additional constraints on the allowable deformation of the ring can increase effective stiffness.

3.3 Parameterized Patterns

Each of our patterns is parameterized to enable user-specified dimensions and stiffnesses. Key parameters include the bending leg height h, the foot width w, length l and hinge joint radius r, all shown in Fig. 5. Fig. 9 shows some examples of different legs achievable using this pattern.

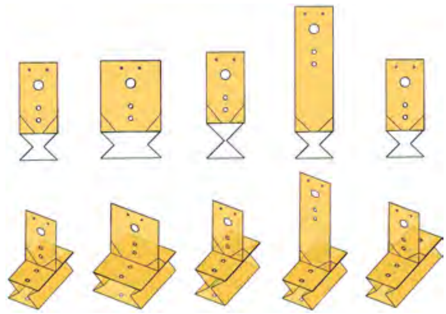

Figure 9: *Front and isometric views of compliant legs with different design parameters. From left to right: original design, larger width, larger r, larger height, and larger length separately from left to right.*

4 Robot Fabrication

We incorporated our compliant leg design into a quadruped robot. Each of the legs was constructed using the pattern shown in Fig 5. We constructed the legs out of 1 mm cardboard, which is low cost and accessible in most local convenience stores. We used multiple layers to increase the stiffness of the bending leg and the rigidity of the top and bottom surfaces of the foot. In Fig 5, layers with same labels overlap.

The feet and compliance modules were assembled using screws through mounting holes at the top and bottom faces (labeled D and R in the diagram). By connecting an additional bending plate to the edges parallel to each of the hinge joints at points C1-4, we achieve elasticity in both prismatic and rotational directions. These two bending plates were made from 22 oz Vinyl Coated Polyester, which had higher durability than the cardboard. To ensure the top and bottom surfaces of the foot remain flat, we attached an additional card stock layer on each side.

Rigid upper legs were constructed from multiple layers of cardboard. The layers were glued together to enhance rigidity. Lower legs were attached to the upper legs using servomotors mounted at M and connected by servohorns at G.

Four legs were attached to a cardboard base using an additional servomotor connected at G to produce a quadruped robot. The total cost of these material was approximately \$2.12. The leg patterns took approximately 6 minutes to be cut by a Vinyl cutter, and 27 minutes to be hand-folded and assembled together into the designed 3D shape. All of the origami components except for the legs were designed to be rigid. The dimensions of the compliant leg are 7.5x5x2.5 cm (height, width, length), while the robot's dimensions are 16.5x17x18.5 cm, with a total mass of 210 g. An on-board micro-controller controlled the robot movement using the gait shown in Fig. 10.

5 Experimental Results

To explore the effect of leg compliance on the quadruped locomotion, we conducted a sequence of static and dynamic tests. Five inertial measurement units (IMU)

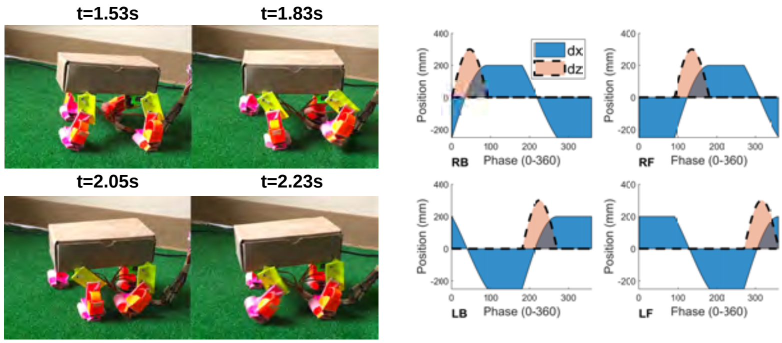

Figure 10: *(left) Snapshots showing the walking gait pattern in a sequential time order. (right) Robot gait broken into sagittal (dx) and vertical (dz) movement for each leg: right back (RB), right front (RF), left back (LB) and left front (LF); dx* > 0 *means step forward and dz* > 0 *means foot lift.*

attached to the body and feet provided measurements of body and ankle orientation as well as linear accelerations. We also designed rigid origami legs with the same dimensions and mass as the compliant legs for comparison (ref. Fig. 1).

5.1 Lateral static perturbation tests

Uneven terrain or obstacles are common sources of perturbation to normal walking cycles. When a rigid robot steps on an unexpected obstacle, its body will tilt around the lowest foot edges. The bending leg is designed to resist the body tilting. To check the resistance of the compliant leg against tilt, we used an IMU to measure the body and ankle tilt of the robot when stepping on obstacles of different sizes. Like Fig. 6b, we placed an obstacle underneath one foot, and we incrementally adjusted the height of the obstacle from 0 to 12 cm. The difference between the ankle and body roll angles provides an indication of the elastic force through deflection; for rigid legs, the ankle and body roll angle are the same.

Fig. 11 shows comparisons of body and ankle roll angle for compliant legs, compliant legs with the additional compliance module (labeled ‘stiffer’), and rigid legs. With compliant legs, the robot’s body rolled less than with rigid legs. In addition, for lower stiffnesses of the leg, both body and ankle roll less, showing that more deformation of the leg occurs. In all cases, the ankles experienced lower roll than the body. The difference between body and ankle roll is due to leg deflection and can be used to approximate the resistive force on the hip for lateral balancing.

5.2 Lateral dynamic stability tests

To test the effect of leg compliance on lateral stability in dynamic locomotion, we made the robot walk forward with a periodic gait. By synchronizing the motion of feet on the same side of the robot, the robot constantly tilted towards the feet with shorter vertical distance to the base. We expect that when the robot with the

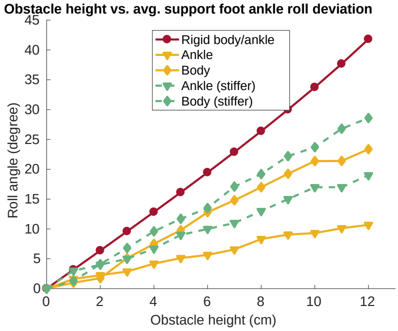

Figure 11: *Body and ankle tilting due to an obstacle placed underneath one foot for compliant legs vs. compliant legs with compliance attachment vs. rigid legs.*

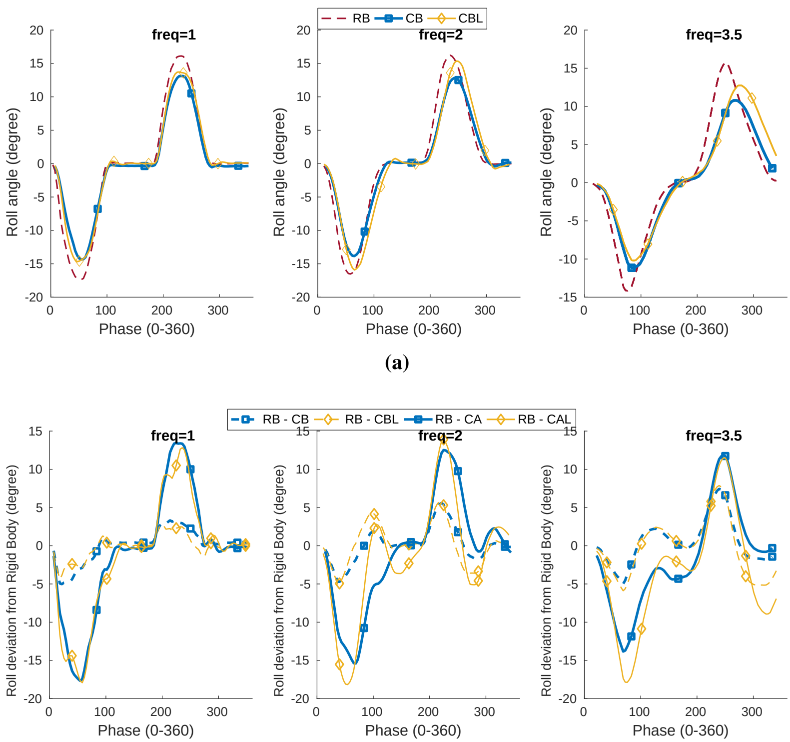

Figure 12: *(a) Comparisons of body roll angles at three different gait frequencies: 1 Hz, 2 Hz, and 3.5 Hz. Rigid body (RB) vs. compliant body (CB) vs. compliant body with external load (CBL); (b) Comparisons of body/ankle roll deviations from the rigid body roll. CA denotes ankle of the compliant robot, CAL denotes ankle of compliant robot with load. Plotted data are mean values sampled from 10 trials.*

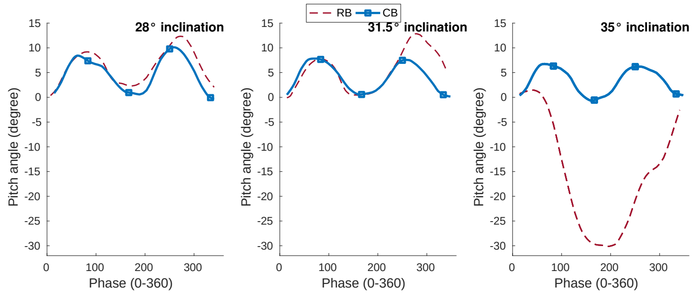

Figure 13: *Comparisons of body pitch, rigid (RB) vs. compliant (CB) robot, during the walking on inclined surfaces with 28, 31.5 and 35 degree of inclination. Data plotted are mean values of data sampled from 10 trials of experiments.*

compliant leg tilts sideways this way, its stance foot will maintain more contact area with the ground and the stance leg will produce higher forces for balance.

In our experiments, we made the robot oscillate at three frequencies 1, 2 and 3.5 Hz. At each frequency, we tested the robot when it was compliant, compliant with an extra load of 280 grams, and rigid without load. The extra load was heavier than the robot's own weight (210 grams) and was placed on top of the robot. We observed the extra load caused the rigid legs to start bending and breaking even at the lowest frequency due to excessive forces overloading the origami structure. Therefore, we do not include roll angle measurements of rigid body with load.

We measured the tilting (roll angle) of the body and all ankles during this motion. Fig. 12a shows comparisons of body roll angles (rigid vs. compliant vs. compliant with load) for each frequency, while Fig. 12b compares the deviations of roll angles (compliant body, compliant ankle, compliant body with load, and compliant ankle with load) from the roll of the rigid body. Due to space limitations, in terms of ankle roll data, we only showed measurements of the right-back (RB) ankle; however, all ankle measurements showed the same trend.

We observe that: 1) at all frequencies, the compliant body tilted less than the rigid body regardless of the external load; 2) at all frequencies, the differences between the rigid body roll and the compliant ankle roll were significantly larger than the differences between the rigid body roll and the compliant body roll, which means the compliant leg deformed and generated spring forces to maintain stability; 3) with an extra load, the robot was more unstable, with the body tilting further from its normal oscillation than without the load; 4) but despite the increased body mass, the robot with compliant legs still outperformed the rigid legs without load. These observations match the expected effect of the origami legs. Compliance in the panels allows them to bend and produce stabler locomotion with greater resistance to body roll. These results are consistent over different gait frequencies.

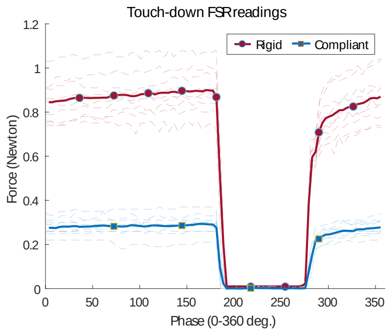

Figure 14: *Mean (solid) impact forces for rigid vs compliant origami leg over multiple experimental trials (dashed).*

5.3 Sagittal dynamic stability tests

To quantitatively measure the resistance to perturbations in the sagittal direction during the normal gait, we made the robot walk over inclined surfaces and compared the differences in terms of body and ankle pitch deviations. We made the robot walk on a flat surface with 28, 31.5, and 35 degrees of inclination. The experimental results are shown in Fig. 13. On the surface with lower inclinations, we observe subtle differences in terms of body and ankle oscillations between the robot with compliant legs and the one with rigid legs. As the angle of inclination increases, these differences increase, creating notable pitch differences between the robot with rigid legs and the one with compliant legs in the last 1/4 of the gait cycle. As the inclination increased up to 35 degrees, the rigid robot became unstable, repeatedly falling backwards, while the compliant one maintains robust locomotion.

5.3.1 Touch-down impacts

To quantitatively understand how the proposed origami leg can reduce impacts, we measured the contact forces for a foot coming into contact with an object when a single leg executes periodic lift-up and step-down motions. The hip was attached to a fixed position while the object was placed right below the hip. When the leg was fully stretched, the foot and obstacle collided. Since we also used the rigid leg for comparisons, in order to prevent damage due to collision, the object we chose was a foam mat. We attached force sensing resistors (FSR) to measure the contact forces between the foot and the fixed object. Compared to the rigid leg of the same design, impact forces between the foot and the ground were reduced by approximately a factor of 3.1 (ref. Fig. 14).

6 Conclusions

In this work, we present our design of an origami-inspired compliant robot leg for stable and robust locomotion. Our proposed leg design consists of multiple elements that combine to produce a leg with three degrees of freedom. The leg leverages material bending and the geometry of the fold pattern to control its compliance. We have integrated this leg into a quadruped robot that can be fabricated and assembled in less than an hour through a cut-and-fold procedure. Our experiments show that the proposed compliant leg design provides enhanced robustness against static perturbations and in dynamic locomotion, as well as reduced foot touch-down impacts, as compared to an equivalent robot with rigid legs.

Future work includes leveraging our reconfigurable compliance module for onsite compliance adaptation. In addition, our dynamical model (ref. sec. 2) indicates we need damping. We would like to include reconfigurable origami-inspired damper for greater robustness of locomotion.

References

[Blickhan and Full 93] Reinhard Blickhan and RJ Full. "Similarity in multilegged locomotion: bouncing like a monopode." *Journal of Comparative Physiology A: Neuroethology, Sensory, Neural, and Behavioral Physiology* 173:5 (1993), 509–517.

[Dai and Cannella 08] Jian S Dai and Ferdinando Cannella. "Stiffness characteristics of carton folds for packaging." *Journal of mechanical design* 130:2 (2008), 022305.

[Deng and Lee 18] Xiang Deng and Daniel D. Lee. "Artificial invariant subspace for humanoid robot balancing in locomotion." In *IEEE/RSJ International Conference on Intelligent Robots and Systems*, p. Under Review, 2018.

[Faal et al. 16] Siamak G Faal, Fuchen Chen, Weijia Tao, Mahdi Agheli, Shadi Tasdighikalat, and Cagdas D Onal. "Hierarchical kinematic design of foldable hexapedal locomotion platforms." *Journal of Mechanisms and Robotics* 8:1 (2016), 011005.

[Greenberg et al. 11] HC Greenberg, Matthew L Gong, Spencer P Magleby, and Larry L Howell. "Identifying links between origami and compliant mechanisms." *Mechanical Sciences* 2:2 (2011), 217–225.

[Holmes et al. 06] Philip Holmes, Robert J Full, Dan Koditschek, and John Guckenheimer. "The dynamics of legged locomotion: Models, analyses, and challenges." *Siam Review* 48:2 (2006), 207–304.

[Li et al. 12] Zhibin Li, Nikos G Tsagarakis, and Darwin G Caldwell. "A passivity based admittance control for stabilizing the compliant humanoid COMAN." In *IEEE-RAS International Conference on Humanoid Robots*, pp. 43–49, 2012.

[Matjačić et al. 01] Z Matjačić, Michael Voigt, D Popović, and Thomas Sinkjær. "Functional postural responses after perturbations in multiple directions in a standing man: a principle of decoupled control." *Journal of Biomechanics* 34:2 (2001), 187–196.

[Mintchev et al. 17] Stefano Mintchev, Sébastien de Rivaz, and Dario Floreano. "Insect-inspired mechanical resilience for multicopters." *IEEE Robotics and Automation Letters* 2:3 (2017), 1248–1255.

[Noh et al. 12] Minkyun Noh, Seung-Won Kim, Sungmin An, Je-Sung Koh, and Kyu-Jin Cho. "Flea-inspired catapult mechanism for miniature jumping robots." *IEEE Transactions on Robotics* 28:5 (2012), 1007–1018.

[Onal et al. 13] Cagdas D Onal, Robert J Wood, and Daniela Rus. “An origami-inspired approach to worm robots.” *IEEE/ASME Transactions on Mechatronics* 18:2 (2013), 430–438.

[Rommers et al. 17] Jelle Rommers, Giuseppe Radaelli, and Just L Herder. “Pseudo-Rigid-Body Modeling of a Single Vertex Compliant-Facet Origami Mechanism.” *Journal of Mechanisms and Robotics* 9:3 (2017), 031009.

[Roy et al. 09] Anindo Roy, Hermano Igo Krebs, Dustin J Williams, Christopher T Bever, Larry W Forrester, Richard M Macko, and Neville Hogan. “Robot-aided neurorehabilitation: a novel robot for ankle rehabilitation.” *IEEE Transactions on Robotics* 25:3 (2009), 569–582.

[Rus and Sung 18] Daniela Rus and Cynthia Sung. “Spotlight on origami robots.” *Science Robotics* 3:15 (2018), eaat0938.

[Saranli et al. 01] Uluc Saranli, Martin Buehler, and Daniel E Koditschek. “Rhex: A simple and highly mobile hexapod robot.” *The International Journal of Robotics Research* 20:7 (2001), 616–631.

[Schulz et al. 17] Adriana Schulz, Cynthia Sung, Andrew Spielberg, Wei Zhao, Robin Cheng, Eitan Grinspun, Daniela Rus, and Wojciech Matusik. “Interactive robogami: An end-to-end system for design of robots with ground locomotion.” *International Journal of Robotics Research* 36:10 (2017), 1131–1147.

[Soltero et al. 13] Daniel E Soltero, Brian J Julian, Cagdas D Onal, and Daniela Rus. “A lightweight modular 12-dof print-and-fold hexapod.” In *IEEE/RSJ International Conference on Intelligent Robots and Systems*, pp. 1465–1471, 2013.

[Sung and Rus 15] Cynthia Sung and Daniela Rus. “Foldable joints for foldable robots.” *ASME Journal of Mechanisms and Robotics* 7:2 (2015), 021012.

[Winter 95] David A Winter. “Human balance and posture control during standing and walking.” *Gait & posture* 3:4 (1995), 193–214.

[Zhakypov and Paik 18] Zhenishbek Zhakypov and Jamie Paik. “Design Methodology for Constructing Multimaterial Origami Robots and Machines.” *IEEE Transactions on Robotics*.

[Zhakypov et al. 17] Zhenishbek Zhakypov, Christoph Belke, and Jamie Paik. “Tribot: A Deployable, Self-Righting and Multi-Locomotive Origami Robot.” In *IEEE International Conference on Intelligent Robots and Systems*, 2017.

Xiang Deng
GRASP Lab, University of Pennsylvania, 3330 Walnut St, Philadelphia, PA 19104, e-mail: dxiang@seas.upenn.edu

Cynthia Sung
GRASP Lab, University of Pennsylvania, 3330 Walnut St, Philadelphia, PA 19104, e-mail: crsung@seas.upenn.edu